

## WATER CLARITY ASSESSMENT FOR A REGIONAL LAKE USING LANDSAT OPERATIONAL LAND IMAGER DATA: A CASE OF NALBAN LAKE IN EAST KOLKATA WETLAND, INDIA

PULAK PRITI PATRA<sup>1a</sup>, SOURABH KUMAR DUBEY<sup>1b\*</sup>, MALANCHA ROY<sup>2b</sup>,  
RAMAN KUMAR TRIVEDI<sup>1c</sup>, SANJEEV KUMAR SAHU<sup>3</sup> AND BASUDEV MANDAL<sup>4</sup>

<sup>1</sup>*Department of Aquatic Environment Management, Faculty of Fishery Sciences, West Bengal University of Animal and Fishery Sciences, Kolkata 700 094, India*

<sup>2</sup>*School of Environmental Studies, Jadavpur University, Kolkata 700 032, India*

<sup>3</sup>*ICAR-Central Inland Fisheries Research Institute, Barrackpore, Kolkata 700 120, India*

<sup>4</sup>*Department of Fisheries Science, Vidyasagar University, Midnapore, West Bengal 721 102, India*

(Received 4 November, 2019; accepted 11 February, 2020)

### ABSTRACT

Landsat operational land imager (OLI) data and consequent laboratory measurements were used to predict water clarity for an inland lake within the East Kolkata Wetland, India (a Ramsar site). Total suspended sediment (TSS) and turbidity was considered as responsible parameters for assessment of lake clarity. The most suitable band ratio was identified by performing Pearson correlation analysis between water clarity concentrations and possible OLI band and band ratios from the 'study points'. The OLI 4 band (636-673 nm) showed the best 'r' value, 0.96 and 0.89 in case of TSS and turbidity respectively. The two separate prediction models (using non-transformed and logarithmically transformed water clarity data) was developed by applying regression analysis between the band reflectance value of OLI4 and water clarity concentrations of the study points. The band reflectance value of the 'validation points' was given as input in the prediction model and model predicted dataset was considered as predicted water clarity parameters. The model predicted dataset exhibit lower standard error of estimates (SEE) with contemporaneous in situ measurements. The validation of the multi-temporal competence of the best models indicated that it is feasible to apply the linear regression model using OLI 4 band to estimate water clarity concentrations across the seasons in Nalban Lake without any in situ data. The water clarity mapping of the lake was then developed using the predicted dataset. This empirical study showed that Landsat 8 OLI imagery could be effectively applied for the mapping of TSS and turbidity for inland lakes.

**KEY WORDS :** Water clarity, Landsat 8 OLI, Nalban Lake, Study points, Validation points, Prediction model

### INTRODUCTION

Water clarity is the measure of transparency level of water, which depends on both colour of water and light scattering. Water clarity has often been used as an indicator of lake's overall water quality as it correlates other water quality variables (Udy *et al.*, 2005). Water turbidity is an optical property of water, which scatters and absorbs the light and

suspended sediments are responsible for most of the scattering (Boyd, 2015). As water turbidity is mainly the result of the presence of suspended matter, turbidity measurement has often been used to calculate fluvial suspended sediment concentrations (Wass *et al.*, 1997) and is commonly regarded as the opposite of clarity. The total suspended solids (TSS) concentration in water can result in high rates of turbidity and sedimentation. Turbidity restricts light

penetration and turbid water with high concentrations suspended soil particles will not be very productive of phytoplankton or other aquatic plants (Scheffer, 1998; Gomez *et al.*, 2004; Boyd, 2015). Suspended materials serve as a carrier and storage agent of pesticides, absorbed phosphorus, nitrogen and organic compounds and can be an indicator of pollution (Jensen, 2000). Nevertheless, turbidity and suspended sediment concentrations of a water body is highly dynamic which influences the species abundance, species composition and total biomass of a lake. Therefore, it is very imperative to monitor and assess the concentrations of suspended materials in lake waters, as well as their spatial and temporal distribution and change.

The traditional method of monitoring water quality is the manual collection of samples from the field and consequent laboratory analysis. Although this in situ measurement offers high accuracy (Ritchie *et al.*, 2003), this process is not suitable to represent a synoptic spatio-temporal water quality database on a regional scale within a short time span and also not effective in terms of operational cost, manpower etc. (Haddad and Harris, 1985; Bhatti *et al.*, 2008; Duan *et al.*, 2013; Lim and Choi, 2015). This problem, however, can be solved by the integration of water quality models, in situ data and remote sensing data, which provide spatially distributed information in a short time span with low operational cost (Zhou *et al.*, 2006; Patra *et al.*, 2017). Since the 1970s, remote sensing techniques have been widely used to monitor inland water quality (Gholizadeh *et al.*, 2016). The satellites engaged in remote sensing are very much effective to measure the optical properties of suspended solids (Duane Nellis *et al.*, 1998). The combination of temporal coverage, spatial resolution, and data availability makes the Landsat system particularly useful for assessment of inland lakes (Kloiber *et al.*, 2002). The 15 and 30 m resolution of the Landsat 8 Operational Land Imager (OLI) combined with high global data availability, present a unique platform to provide the first and most up-to-date global inventory of the world's lakes and water quality information retrieval at high spatial resolution and positional accuracy using recent Landsat algorithms (Smith *et al.*, 2005; Sheng and Li, 2011; Li and Sheng, 2012). Miller *et al.*, (2013) opined that the Landsat series provided approximately \$2.19 billion economic advantage per year that had been expended over several fields of research.

Remote sensing techniques are widely used to

estimate and map the turbidity and concentrations of suspended particles, and to provide their spatial and temporal variations. The common method applied in previous studies involved the regression analysis of Landsat data and roughly contemporaneous ground observation data. Several investigations established reliable empirical relationships between Landsat Multispectral Scanner (MSS), Thematic Mapper (TM), Enhanced Thematic Mapper Plus (ETM+) data and ground observations of suspended matter or turbidity (Khorram *et al.*, 1991; Cox *et al.*, 1998; Zhou *et al.*, 2006; Wang *et al.*, 2004; Papoutsas *et al.*, 2014; Lim and Choi, 2015) employing signal band or band ratios.

The overall objective of this study was to develop a method for using Landsat-8 OLI imagery data to estimate TSS and turbidity concentrations in Nalban Lake, East Kolkata Wetland (EKW), West Bengal, India. The study also optimized the suitable OLI band for forecasting water clarity and developed optimized prediction models regionally.

## Description of the study area

### The Nalban Lake

The Nalban Lake is a part of the large-scale wastewater-fed aquaculture system, the East Kolkata Wetland (EKW) (latitude 22°25' – 22°40' N, longitude 88°20' – 88°35' E). The EKW was considered as “Wetland of International Importance” under the Ramsar Convention on August 19, 2002 due to its wise use of wetland. The waste recycling region is located at the eastern part of peri-urban Kolkata city, West Bengal, India (Fig. 1). Out of the designated 12500 ha of areas, the wastewater-fed aquaculture impoundments cover roughly 3900 ha and the fish production varies from 3.0 to 6.0 tons ha<sup>-1</sup> year<sup>-1</sup>. The Nalban Lake is rain fed; semi-closed type and water spread area is about 126 ha. Aquaculture activities continue throughout the year and fishes comprising carps, catfishes, and tilapia are the major produce sold in local as well as in distant market. This lake is now under the administrative control of State Fisheries Development Corporation Ltd, Government of West Bengal.

### Water sampling procedure

The in situ sampling was performed on the prefixed date when Landsat satellite overpasses the Kolkata city region. The water sampling procedure was

done in two phases and was restricted to surface water. In the first phase, eight sampling sites (S1-S8) were selected encompassing the entire lake surface area. These eight points were considered as ‘study points’ (Figure 1). A single study point was sampled once only on the date of satellite overpass day. It took three months to complete the sampling process for all the eight study points.

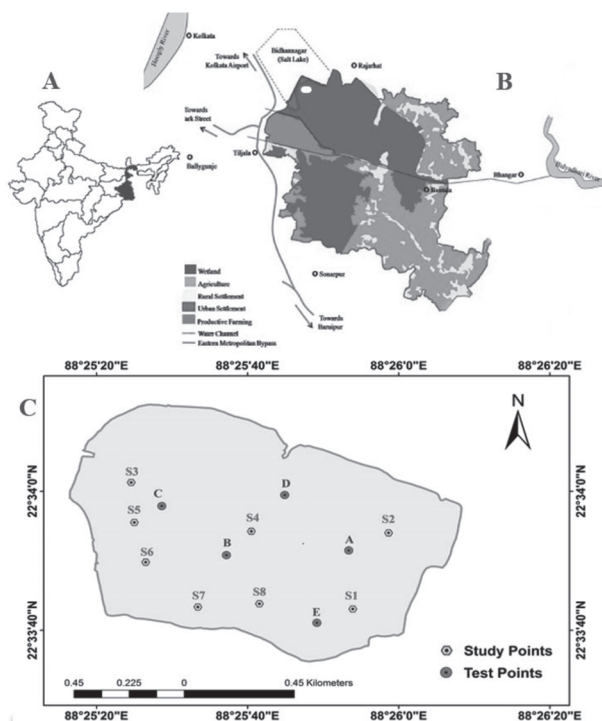


Fig. 1. Location map of the study area. A India, B East Kolkata Wetland and C Nalban Lake.

Water samples were collected in amber bottles and were brought immediately to the laboratory for further analysis. The amount of suspended solid (TSS) in the sample water was quantified by filtering sample through a tared glass fiber filter, the

filter and residue were dried at 102° C, and the weight gain of the filter was caused by the suspended solids retained on it (Boyd 1998). The turbidity of the sample water was estimated following the nephelometric method by comparing the intensity of light scattered by sample under defined condition with the intensity of light scattered by a standard reference suspension (Formazin suspension) (Eaton *et al.*, 2005) by using a nephelometer (Systronics; Model: MK-132). The turbidity is expressed as nephelo turbidity unit (NTU). The TSS concentration and the turbidity of each study points are tabulated in Table 1. The data obtained from these study points were considered as primary data for establishment of the prediction model.

In the next phase, five ‘validation points’ were randomly selected from the lake surface (Figure 1) (Table 2). The sampling procedures were repeated for these five specific points on each satellite-passing day and followed by same TSS concentration and the turbidity estimation method. The sampling procedures were carried on 9<sup>th</sup> March, 24<sup>th</sup> March, 25<sup>th</sup> April, 11<sup>th</sup> May and 27<sup>th</sup> May 2015. These dataset was used for the validation of pre-established TSS and turbidity model for the lake. The co-ordinates of the both the study points and validation points were geo-located with the help of a hand held GPS recorder (Garmin eTrex<sup>®</sup> 10).

**Lands at 8OLI Data**

The cloud-free ‘Landsat 8 OLI’ satellite images have been used in the present study. It is an Earth observation satellite that was launched on February 11, 2013 from California, USA. This new Landsat Misson is controlled by two organizations the United States Geological Survey (USGS) and the National Aeronautics and Space Administration

**Table 1.** Laboratory-measured Total Suspended Solids (TSS) and turbidity concentration of the study points in Nalban Lake

Station	Sampling Date	Geo-coordinates		TSS (mg L <sup>-1</sup> )	Turbidity (NTU)
S1	16 November 2014	22°33'43.06"N	88°25'53.92"E	260	14
S2	2 December 2014	22°33'54.02"N	88°25'58.66"E	295	15.5
S3	18 December 2014	22°34'1.29"N	88°25'24.60"E	265	13.3
S4*	03 January 2015	22°33'54.25"N	88°25'40.50"E	265	14.2
S5*	19 January 2015	22°33'55.52"N	88°25'25.01"E	275	14.5
S6	4 February 2015	22°33'49.80"N	88°25'26.51"E	290	15.3
S7	20 February 2015	22°33'43.34"N	88°25'33.42"E	265	13
S8	8 March 2015	22°33'43.82"N	88°25'41.56"E	280	13.8

\*These two study point data were excluded due to > 50% cloud coverage in Landsat scenes

**Table 2.** Pearson correlation coefficient ( $r$ ) between Total Suspended Solids (TSS) concentration and various Landsat OLI bands and band ratios of the study points

Band Ratio	Correlation coefficient ( $r$ )	Band Ratio	Correlation coefficient( $r$ )
B2	0.85	(B3+B5)/2	0.94
B3	0.92	(B2+B5)/2	0.89
<b>B4</b>	<b>0.96</b>	(B4+B3)/2	0.95
B5	0.89	(B4+B2)/2	0.91
B5/B2	-0.36	(B3+B2)/2	0.89
B5/B3	-0.5	(B2+B3+B4)/3	0.92
B5/B4	-0.11	(B2+B3+B5)/3	0.91
B4/B3	-0.5	(B3+B4+B5)/3	0.95
B4/B2	-0.35	(B2+B4+B5)/3	0.91
B3/B2	-0.24	(B2+B3+B4+B5)/4	0.92
(B4+B5)/2	0.93		

The bold indicates highest correlation

(NASA) by partnership basis (Irons and Loveland 2013). Landsat-8 satellite carries two sensor payloads, the Operational Land Imager (OLI) and the Thermal Infrared Sensor (TIRS). The Landsat 8 OLI exhibits a higher resolution wavelength coverage than the Landsat 7 ETM+ bands due to the addition of a new coastal/aerosol band (0.43–0.45  $\mu\text{m}$ ) for detecting suspended solids and a new cirrus band (1.36–1.39  $\mu\text{m}$ ) for detecting clouds (Roy *et al.*, 2014). Addition of new coastal/aerosol band (0.43–0.45  $\mu\text{m}$ ) for detecting suspended solids and new cirrus band (1.36–1.39  $\mu\text{m}$ ) for retrieving clouds has increased the resolution and make it more efficient than the ETM+(Roy *et al.*, 2014). The satellite images used in this study were downloaded from the archive of USGS Landsat images (<http://earthexplorer.usgs.gov/>). This study utilized visible bands (blue, green, and red) and a near-infrared (NIR) band to determine correlations between water

clarity and spectral reflectance values. All image data from the Landsat 8 OLI were in GeoTIFF format provided by the US Geological Survey Earth Explorer. The details of Landsat bands used for model development were presented in Table 3. Scenes greater than 50% cloud coverage was excluded from model development. For the validation of the model, three Landsat scenes, 24<sup>th</sup> March, 25<sup>th</sup> April and 27<sup>th</sup> May 2015 were used.

## MATERIALS AND METHODS

### Processing of satellite data

#### DN value extraction and conversion to TOA reflectance data

The digital number (DN) value was extracted from the satellite images for the coordinates of study points and validation points respectively with the

**Table 3.** Pearson correlation coefficient ( $r$ ) between turbidity concentration and various Landsat OLI bands and band ratios of the study points

Band Ratio	Correlation coefficient ( $r$ )	Band Ratio	Correlation coefficient( $r$ )
B2	0.85	(B3+B5)/2	0.87
B3	0.81	(B2+B5)/2	0.87
<b>B4</b>	<b>0.89</b>	(B4+B3)/2	0.88
B5	0.86	(B4+B2)/2	0.84
B5/B2	-0.5	(B3+B2)/2	0.86
B5/B3	-0.42	(B2+B3+B4)/3	0.86
B5/B4	0.06	(B2+B3+B5)/3	0.86
B4/B3	-0.5	(B3+B4+B5)/3	0.88
B4/B2	-0.5	(B2+B4+B5)/3	0.88
B3/B2	-0.5	(B2+B3+B4+B5)/4	0.87
(B4+B5)/2	0.88		

The bold indicates highest correlation

help of TNT MIPS 2013 software (Version 15.0.0.533). The raw DN value was converted into top of atmosphere (TOA) planetary reflectance ( $\rho^\lambda$ ) using the rescaling co-efficient supplied with image metafile. Equation 1 obtained from ([http://landsat.usgs.gov/Landsat8\\_Using\\_Product.php](http://landsat.usgs.gov/Landsat8_Using_Product.php)) was used for the conversion process.

$$\rho^\lambda = M_p * Q_{cal} + A_n \quad ..(1)$$

Where,

$\rho^\lambda$  = TOA planetary reflectance, without correction for solar angle

$M_p$  = Band specific multiplicative rescaling factor from metadata

$A_n$  = Band specific additive rescaling factor from metadata

$Q_{cal}$  = Quantized and calibrated standard product pixel value

The TOA reflectance values were further rectified taking into account that water leaving radiance greatly varies depending on the solar angle. The value of local solar zenith angle and local sun elevation angle was taken from the metadata file provided with the Landsat data. The equation 2 obtained from ([http://landsat.usgs.gov/Landsat8\\_Using\\_Product.php](http://landsat.usgs.gov/Landsat8_Using_Product.php)) was used for sun angle correction.

$$\rho\lambda = \rho^\lambda / \cos(\theta_{sz} * \pi/180) = \rho^\lambda / \sin(\theta_{se} * \pi/180) \quad ..(2)$$

Where,

$\rho\lambda$  = TOA planetary reflectance

$\theta_{se}$  = Local sun elevation angle

$\theta_{sz}$  = Local solar zenith angle

### Atmospheric Correction

For routine monitoring of water quality parameters from remotely sensed imagery data, suitable atmospheric correction is very much important (Hu *et al.*, 2004). The different atmospherically influenced phenomenon (e.g. scattering, absorbing and refracting light) affects satellite images (Chavez, 1988). In this study, darkest pixel (DP) atmospheric correction method (histogram minimum method) was applied (Hadjimitsis *et al.*, 2004a) and previous studies confirmed that the DP atmospheric correction method is the most suitable for inland waters (Hadjimitsis, 1999; Hadjimitsis *et al.*, 2004b). This method assumes that any dark pixel on the scene that possesses the lowest DN value should have a zero reflectance. Therefore, its radiometric DN value represents the atmospheric additive effect

(Crane, 1971; Crippen, 1987; Campbell, 2008). In the DP atmospheric correction method, from a dark object, the atmosphere at visible wavelengths affects most of the signal reaching a satellite sensor. Therefore, the amount of upwelling path radiance in each band can be measured from the pixel that is considered as dark targets on the satellite image. Since the atmospheric path radiance affects the surface radiance of the dark target, the radiance resulting from the corresponding pixels is considered proportional to the atmospheric path radiance and can be used to account for the additive effect of atmospheric scattering (Wu *et al.*, 2005). Therefore, the minimum DN value in the histogram is subtracted from all pixels within the scene.

### Development of regression based prediction model

Statistical techniques like correlation and regression have been the most commonly used approach to derive relation between spectral data and total suspended matter and turbidity concentration (Zhou *et al.*, 2006). The Pearson correlation analysis was performed between possible bands/band combinations and the in situ water quality measurement (TSS and turbidity) of the study points to examine the relationship. Previous studies suggest that different band combinations (e.g. ratios, multiplication and average) which can be used to retrieve relationships with in-situ measurements (Lathrop, 1992; Lavery *et al.*, 1993; Kloiber *et al.*, 2002). Prediction models were then developed using the linear regression analysis. The regression relationship between water quality parameters and the corresponding reflectance values of remotely sensed imagery can be simple linear, multiple linear or nonlinear (Lopez-Garcia and Caselles, 1987; Lathrop and Lillesand, 1989; Lathrop, 1992; Aguirre-Gomez, 2000), however, linear type of regression is effective in inferring turbidity despite possible variation in water constituents and impact of bottom reflectance (Fraser, 1998).

### Accuracy assessment of the model

To check the efficiency and prediction accuracy of the models, the validation process was performed. The reflectance value of the validation points at the predictive band or band combination was given as input in the developed model and the model generated output values were considered as predictive water quality. Statistical metrics like SEE (Standard Error of Estimates) and RMSE (Root

Mean Square Error, in log space) was used to evaluate the efficiency of the predictive models (IOCGC, 2006; McHugh, 2008).

The SEE is a measure of the accuracy of predicted scores in a regression. If SEE value is small, it would therefore expect that most of the observed values cluster fairly closely to the regression line. It was calculated by the following formula

$$\sigma_{Est} = \frac{\sqrt{\sum(Y-Y')^2}}{N} \quad .. (3)$$

Where,  $\sigma_{Est}$  is the SEE,  $Y$  is an actual score,  $Y'$  is a predicted score, and  $N$  is the number of pairs of scores.

The RMSE is a measure of the average magnitude of the error. Its value ranges from 0 to  $\infty$ . Lower values of RMSE indicate better fit. RMSE is a good measure of how accurately the model predicts the response and is the most important criterion for fit if the main purpose of the model is a prediction. It was calculated by the following formula.

$$RMSE = \sqrt{\frac{\sum_{i=1}^n [\log(x_i^{estimated}) - \log(x_i^{measured})]^2}{n-2}} \quad .. (4)$$

Where,  $x_i^{measured}$  represents measured in situ water quality data at the validation sites and  $x_i^{estimated}$  is the model estimated water quality and  $n$  is the number of validation points.

### Data Analysis

The satellite imagery data was processed with the help of the TNT MIPS 2013 (Ver 15.0.0.533) software. For establishing the model, the statistical analysis was performed by IBM SPSS 20.0 statistical software. The boundary map of the study area and spatial maps were prepared through ArcGIS software (10.2.2). The graphs and plots were generated using statistical software Origin® version 6.1 (Origin Lab Corporation, Northampton, USA). The entire approach and methodologies followed in the study was adopted from authors' previous study on prediction of chlorophyll-a concentration (Chl-a) and the trophic states through Landsat 8 OLI data for same lake after some modification (Patra *et al.*, 2017).

## RESULTS AND DISCUSSION

In situ measured TSS concentrations of the lake varied during the entire study period and ranged from 260 to 290 mg L<sup>-1</sup>. The highest value of TSS was observed in study point 'S2' which was sampled on

December 2014 and the lowest in study point 'S1' sampled on November 2014. The turbidity level in the Lake ranged from 13 NTU to 15.5 NTU. The highest value of turbidity was observed in study point 'S2' which was sampled on December 2014 and the lowest in study point 'S7' sampled on February 2015.

### Development of prediction model

The Landsat visible bands ranging from blue (OLI 2) to green (OLI 4) and near-infrared band (NIR) (OLI 5) are commonly used for lake study and applied to obtain the relationship between the sub-surface reflectance and the bio-physical parameters (e.g. water transparency, Chl-a and total suspended solids etc.) of the water (Topliss *et al.*, 1990; Yuming and Min, 1992; Sass *et al.*, 2007; Doxaran *et al.*, 2009). Pearson correlation analysis was performed to observe the relative strengths between TSS and turbidity concentration and OLI bands (2-5) and their combinations of the study points. The Pearson correlation coefficients ( $r$ ) between TSS and turbidity concentration and various Landsat OLI bands and band ratios of the study points were depicted in Table 2 and 3 respectively. The red band-B4 (636-673nm) demonstrated strongest correlation with TSS ( $r = 0.96$ ;  $p < 0.05$ ) and turbidity ( $r = 0.89$ ;  $p < 0.05$ ). So, this band was chosen further for model development.

Linear regression analysis was then performed between atmospherically corrected spectral reflectance values at red band (B4) and the in-situ measured TSS and turbidity dataset of the study points for the development of prediction models. The regression analysis between TSS concentration and spectral reflectance values at red band (B4) demonstrated a significant relationship ( $R^2 = 0.92$ ) with an SEE of 4.43 mg L<sup>-1</sup>. Likewise, the regression analysis between turbidity value and spectral reflectance values at red band (B4) demonstrated a positive relationship ( $R^2 = 0.80$ ) with the SEE of 0.50 NTU. The fitted regression line and its confidence and prediction bands at the confidence level of 95% are shown in Figure 2 and Figure 3. Equation 5 presented the prediction model for TSS whereas equation 6 is considered for prediction of turbidity.

$$TSS_c = a + b (OLI 4) + c \quad .. (5)$$

Where,  $TSS_c$  is the concentration of TSS (mg L<sup>-1</sup>); OLI 4 is the atmospherically corrected band reflectance value and  $a$  and  $b$  are the regression coefficients, equal to 240.3 and 1228 mg L<sup>-1</sup>

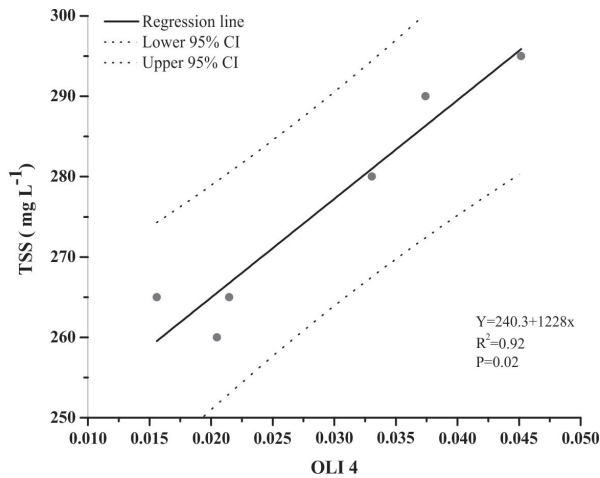


Fig. 2. Fitted regression line between Total Suspended Solids (TSS) and OLI 4 at the confidence level of 95%.

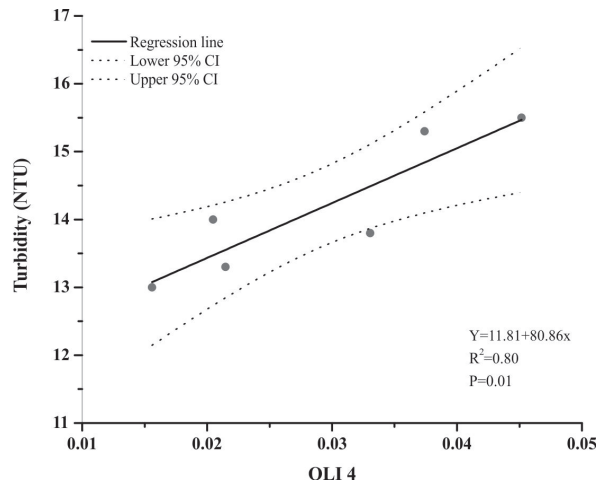


Fig. 3. Fitted regression line between turbidity and OLI 4 at the confidence level of 95%.

respectively.

$$T_c = a + b(\text{OLI } 4) + c \quad \dots (6)$$

Where,  $T_c$  is the concentration of turbidity (NTU); OLI 4 is the atmospherically corrected band reflectance value and  $a$  and  $b$  are the regression coefficients, equal to 11.81 and 80.86 NTU respectively.

Previous studies showed that single band algorithms might be adopted where total suspended matters increases with increasing reflectance (Curran *et al.*, 1987; Novo *et al.*, 1989; Dekker *et al.*, 1993). However, presence of complex substances in water change the reflectance of the water body and therefore cause variation in colors, and thus, different spectral bands can be used for TSS

retrievals (Giardino *et al.*, 2001; Wang *et al.*, 2004; Nechad *et al.*, 2010; Feng *et al.*, 2014). Several studies have also found that the first four bands of Landsat (blue, green, red and NIR) are well correlated with total suspended matters (Cox *et al.*, 1998; Dekker *et al.*, 2001; Dekker *et al.*, 2002; Kloiber *et al.*, 2002; Brezonik *et al.*, 2005; Sudheer *et al.*, 2006). This result is well consistent with several previous investigations (Ritchie *et al.*, 1987; Bilge *et al.*, 1997; Tassan, 1997; Dekker *et al.*, 2002) which showed that TM 3 (red band) (630 to 690 nm) can provide valuable information when large sediment loads occur in lake water and are specially useful for the quantification total suspended matter in shallow lakes. Zhou *et al.*, (2006) also found that TM 3 (red band) is the best predictor of total suspended matter in Lake Taihu, China at different seasons. The red portion of the visible spectrum (for example Landsat TM3; 600–700 nm) is most appropriate for estimating concentrations of suspended matter in inland waters as scattering from suspended materials dominates the reflectance spectra when compared to pure water and phytoplankton absorption (Kirk, 1994, Mobley, 1994, Miller and McKee, 2004; Zhou *et al.*, 2006). However, Ritchie *et al.*, (1976) by in situ studies showed that the most useful range of spectrum for the determination of suspended particles in surface waters was between 700 and 800 nm. Lim and Choi, (2015) also correlated suspended solid concentration with Bands OLI 2- OLI 5 and constructed multiple regression models of three bands.

Band composition ranged from 1 to 7 of Landsat TM satellite image and their combinations was generally useful to retrieve different level of turbidity (He *et al.*, 2008; Alparslan *et al.*, 2009). Generally, in case of low to moderate turbidity values, satellite bands located at red part of the spectrum exhibit good correlation. In consistent to the present study, Landsat TM3 (red band) has been successfully used to map turbidity in Guadalquivir River (Spain) for a turbidity range 1.5-8 NTU (Bustamante *et al.*, 2009). Choubey, (1992) also reported strong correlation ( $r = 0.88$ ) between LISS-I red band (620–680 nm) and turbidity ranged 15–45 NTU in the Tawa reservoir in India. Goodinet *et al.*, (1996) used SPOTHRV2 red band (610–680 nm) spectrum to retrieve relatively low levels of turbidity (3 to 15 NTU) in the Tuttel Creek reservoir of USA. Similarly, MODIS 250-m resolution band at 645 nm was applied to map turbidity ranged between 0.9-8.0 NTU in the Tampa Bay (USA) (Chen

*et al.*, 2007). Petus *et al.*, (2010) developed an empirical predictive algorithm model for turbidity varied from 0.5 to 70.0 NTU using MODIS-Aqua 250- m red band at the Adour River plume (Bay of Biscay, France). A multiple linear regression analysis using Landsat red (630–690 nm) and near infrared (750–900 nm) bands was used by Liversedge, (2007) to predict turbidity in a glacial lake of Alaska where turbidity varied between 2–997 NTU. Papoutsas *et al.*, (2014) also found statistical correlation between in-situ turbidity values and Landsat TM 3 (red band) mean reflectance values, with resulting high  $r$ -value (0.92) at Asprokremmos Reservoir, Cyprus.

We further critically assessed the algorithm models for supplement any accuracy factors that can produce better models with precision. Therefore, while checking the residual output of regression model, we observed a weak and non-random distribution of the residuals versus fitted

value plot (Figure 4a and Figure 4b). This pattern suggested that an exponential function rather than a linear type might improve the relationship between TSS and turbidity value with OLI 4 (Zhou *et al.*, 2006). Thus, we logarithmically transformed the TSS and turbidity concentrations, and employed another linear model as described by Zhou *et al.*, (2006). The plot of residual versus fitted values (Figure 5a and Figure 5b) indicated that, subsequent transformation, the residuals are randomly distributed and SEE has been decreased. The fitted regression line and its confidence and prediction bands at the confidence level of 95% are shown in Figure 6 and 7. The modified forms of TSS and turbidity prediction equations are

$$\log_{10} \text{TSS}_c = a + b (\text{OLI } 4) + c \quad \dots (7)$$

Where  $a$  and  $b$  are equal to 5.49 and 4.42, respectively and SEE decreased to 0.01 mg/L.

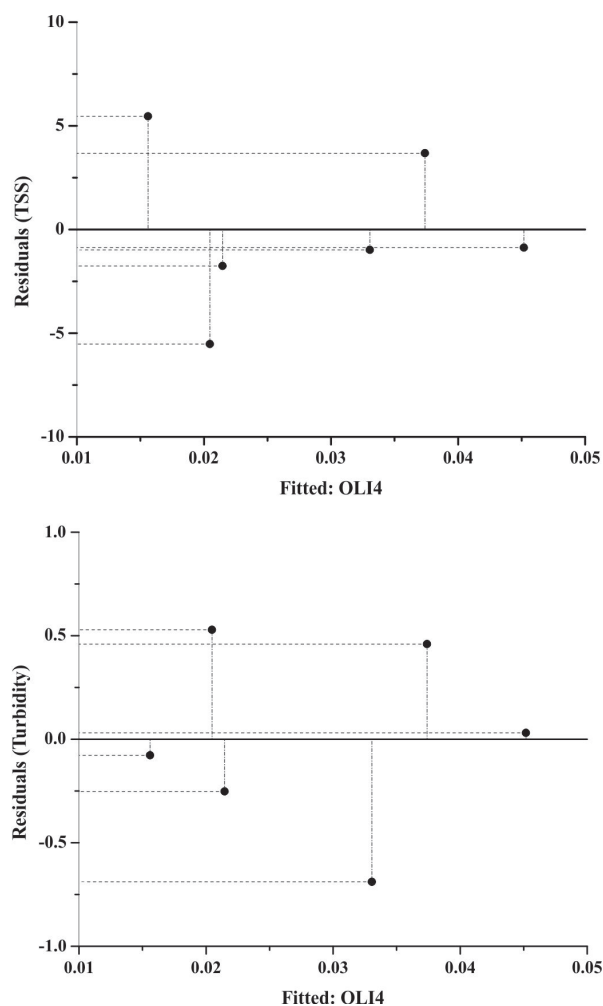


Fig. 4. Residuals versus fitted value plot of a) Total Suspended Solids (TSS) and b) turbidity.

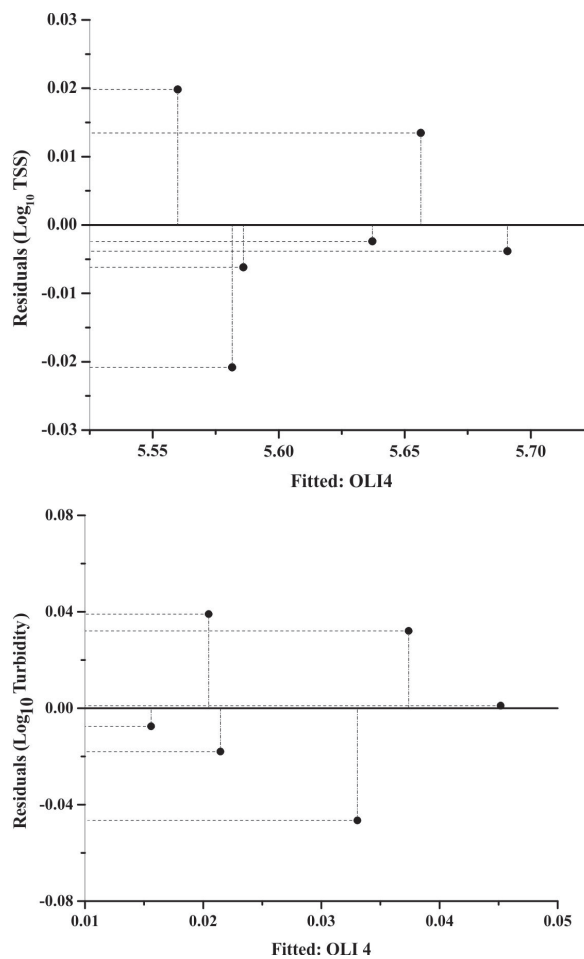


Fig. 5. Residuals versus fitted value plot of logarithmically transformed a) Total Suspended Solids (TSS) and b) turbidity.

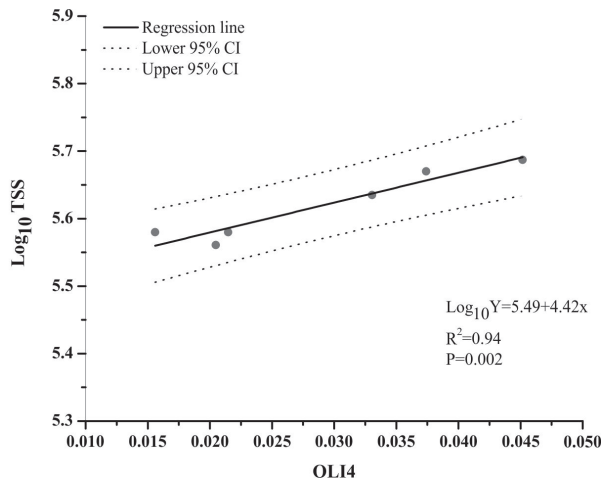


Fig. 6. Fitted regression line between logarithmically transformed Total Suspended Solids (TSS) and OLI 4 at the confidence level of 95%.

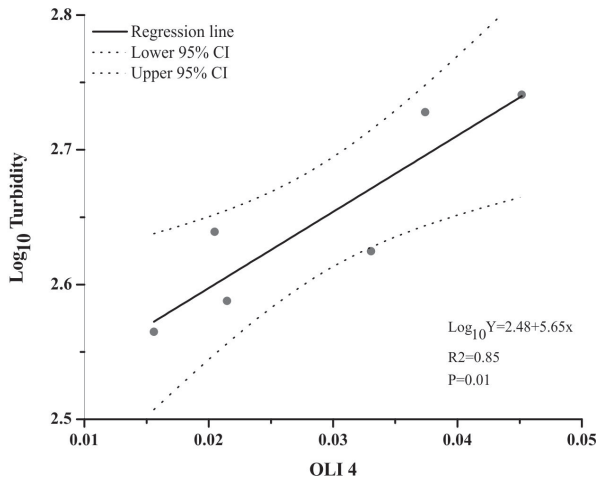


Fig. 7. Fitted regression line between logarithmically transformed turbidity and OLI 4 at the confidence level of 95%.

$$\log_{10} T_c = a + b (\text{OLI } 4) + c \quad \dots (8)$$

Where *a* and *b* are equal to 5.65 and 2.4, respectively and SEE decreased to 0.03 NTU.

**Validation of the prediction model**

We validated the temporal capability of the models in order to get a season-consistent model that had the ability to predict water clarity in multiple seasons. The validation data were different from the model building data. In this experiment, Landsat scenes of March, 2015, April 2015 and May 2015 were used.

The reflectance value at OLI 4 band of the validation point co-ordinates were given as input in equations (5) to (8) and the output data were

considered as predicted dataset. The results indicated that logarithmically transformed model (equation 7 and 8) is the significant predictor of water clarity. The comparison of the estimated TSS and turbidity concentrations with in situ sample data of validation point is shown in Figure 8 and Figure 9. The TSS concentration and model-fitted TSS value of the validation points revealed an SEE of 0.05 (mg L<sup>-1</sup>) with an RMSE of 0.05. In case of turbidity, the regression analysis between model predicted dataset and ground survey dataset value of the validation points generated an SEE of 0.07 (NTU) an RMSE of 2.85. Therefore, the model using B4 band has multi-temporal utility, and can be applied to estimate TSS and turbidity concentrations in different seasons for Nalban Lake.

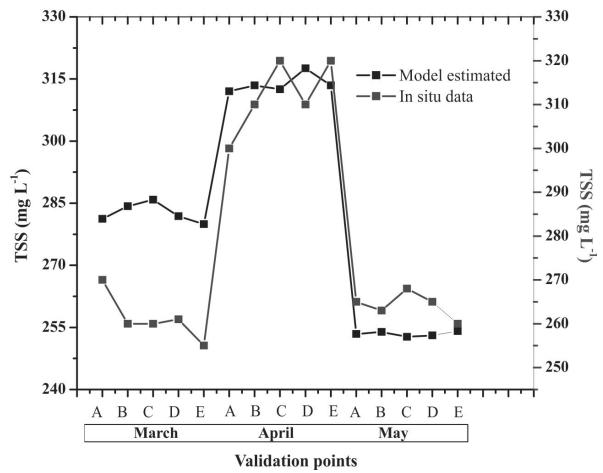


Fig. 8. Comparison of the OLI 4-derived Total Suspended Solids (TSS) estimates with in situ sample data, using equation (7) of the validation points.

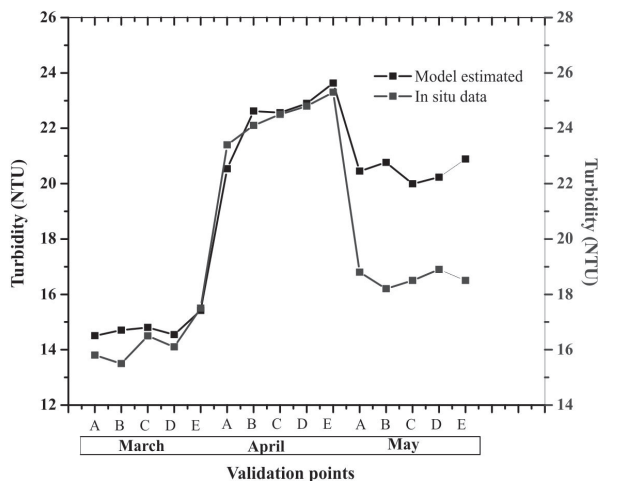


Fig. 9. Comparison of the OLI 4-derived turbidity estimates with in situ sample data, using equation (7) of the validation points.

The regression analysis using equation 5 and 6 yielded high SEE and RMSE value and thus not suitable for model prediction. In consistent to the study, Wang *et al.*, (2016) also found a stable predicted value of TSS concentration applying logarithmic transformed model using red band and NIR band of Landsat OLI. Khorram and Cheshire (1985) found RMSE value of 0.5 NTU and 2.79 mg L<sup>-1</sup> respectively between model predicted and in-situ measured values of turbidity and TSS during study with Landsat Multispectral Scanner (MSS) data at Neuse River Estuary, North Carolina. Keith *et al.*, (2014) empirically developed a water clarity algorithm by regressing in situ turbidity measured from Pensacola Bay against remotely sensed reflectance values retrieved at 646 nm (Red band) from a HICO image (Hyperspectral Imager for the Coastal Ocean). The model was validated in St Andrews Bay and Choctawhatchee Bay and results showed a strong relationship ( $R^2 = 0.67$ ; RMSE = 0.56 NTU) between measured and predicted values. Lim and Choi, (2015) measured *in-situ* concentration of TSS such as 7.3 mg L<sup>-1</sup>, 7.3 mg L<sup>-1</sup> and 6.1 mg L<sup>-1</sup> and the predicted value using Landsat 8 OLI was 5.62 mg L<sup>-1</sup>, 4.58 mg L<sup>-1</sup>, 5.5 mg L<sup>-1</sup> in River Nakdong, Korea.

### Spatial pattern of TSS and turbidity in Nalban Lake

The TSS (equation 7) and turbidity (equation 8) prediction model was applied to the Landsat-8 OLI data of three consecutive month viz., March 2015, April 2015 and May 2015. The resulting thematic maps of TSS and turbidity concentration level of Nalban Lake are shown in Figure 10 and Figure 11. The dynamic maps indicated a higher concentration

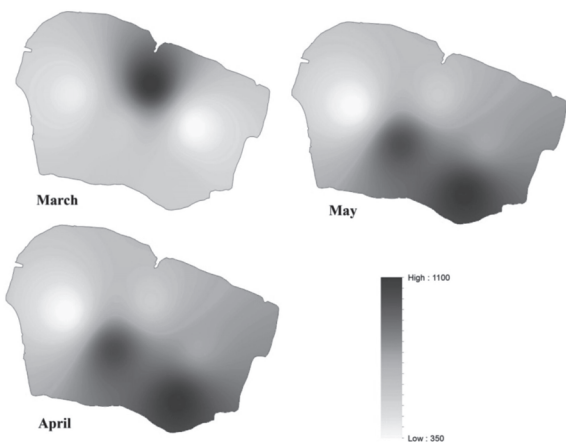


Fig. 10. Spatial pattern of Total Suspended Solids (TSS) concentration in Nalban Lake on 2015.

(>550 mg L<sup>-1</sup>) of TSS in the middle and southeast part of the lake. Probably the strong wind action in the middle of the lake is the responsible for the massive re-suspension of bottom material resulting high TSS concentration (Zhou *et al.*, 2006). The concentration of suspended sediment is relatively higher at the entire eastern region than the western part of the lake. This is due to presence of inlet of a sewage water channel. In the month of April, the higher concentration of TSS has been found in northern part of the lake. As this portion of the lake is shallow and regularly used as fish harvesting, the loose sediment easily floats up in the windy days. Another possible cause may be the anthropogenic activities, as there is a recreational park and settlement on that side of the lake. Nevertheless, the eastern portion of the lake exhibit low TSS level as this portion is relatively less disturbed area due to less human intervention.

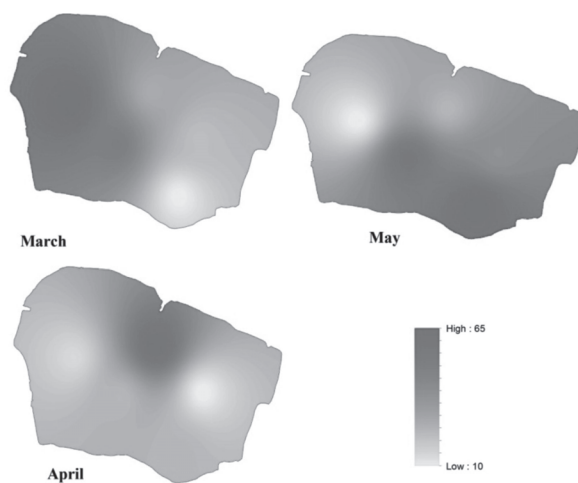


Fig. 11. Spatial pattern of turbidity concentration in Nalban Lake on 2015.

Generally, water turbidity is influenced by several factors such as urban development, human activities, agricultural runoff and recreational activities. Besides that, the chlorophyll concentration is also an important factor that decides the turbidity level of the water body (Patra *et al.*, 2017). Western side of the lake exhibit higher turbidity level than eastern side. Patra *et al.*, (2017) found higher concentration of Chl-*a* concentration on March 2015 on the western side. Therefore, Chl-*a* is responsible for the elevated turbidity level in the western bank of the lake. As TSS level is high in the mid-northern part, the turbidity level in that part is also higher.

## CONCLUSION

This study established a procedure to estimate and map the water clarity (TSS and turbidity) concentrations in inland water by developing and applying regression models to Landsat 8 OLI imagery, taking Nalban Lake, EKW as a case study. The method presented in this paper can be employed to evaluate and map the spatial patterns of suspended sediment concentrations using multi-spectral imagery. As a good harmony between satellite-estimated and measured values of water clarity variables were observed, the study proved that Landsat 8 OLI data is well suited for the study of suspended matter and turbidity in inland lake waters. Results summarized that the red band (B4) is the best predictor of TSS and turbidity concentration in the different seasons for the Nalban Lake. The great advantage of using satellite imagery is the capability of their multi-temporal application covering a large area and low costs compared to laboratory analysis for the evaluation of the water clarity over several lakes. The present findings can support a decision regarding water resources management, water preservation and aquaculture operations in that lake. As the suspended sediment concentrations is tend to high at the Nalban Lake, this study suggests long-term monitoring of water quality conditions and recommends implementing suitable management plans to sustain the aquaculture and other activities over the lake. Further fine tuning of raw image data from the Landsat 8 OLI sensor through calibration and validation and further long-term research using remote sensing technologies will enable improvement of results in water quality of the Nalban Lake as well as East Kolkata Wetland, India.

## ACKNOWLEDGEMENTS

The authors would like to acknowledge ICAR-Central Fisheries Research Institute, Barrackpore for helping in analyzing the satellite data. We are also thankful to General Manager, SFDC for giving permission to carry out research work in Nalban Lake.

**Disclosure statement:** No potential conflict of interest was reported by the authors.

## REFERENCES

- Aguirre-Gomez, R. 2000. Detection of total suspended sediments in the North Sea using AVHRR and ship data. *Int. J. Remote. Sens.* 21(8) : 1583-1596.
- Alparslan, E, Coskun, H.G. and Alganci, U. 2009. Water Quality Determination of K c k kmece Lake, Turkey by Using Multispectral Satellite Data. *The Scientific World Journal.* 9 : 1215-1229.
- Bilge, F., Dogeroglu, T. and Ayda, C. 1997. Mapping of water quality parameters by using Landsat images in Porsuk Dam Lake, Eskisehir, Turkey p.101-107. In: Yilmazer, I. (ed) *Proceedings of the International Symposium on Geology and Environment*, Turkey.
- Boyd, C.E. 1998. *Water Quality for Pond Aquaculture*. Auburn University, Alabama.
- Boyd, C.E. 2015. *Water Quality, An Introduction*. Springer, New York.
- Brezonik, P., Menken, K.D. and Bauer, M. 2005. Landsat-based Remote Sensing of Lake Water Quality Characteristics, Including Chlorophyll and Colored Dissolved Organic Matter (CDOM). *Lake and Reservoir Management.* 21(4) : 373-382.
- Bustamante, J., Pacios, F., D az-Delgado, R. and Aragone´s, D. 2009. Predictive models of turbidity and water depth in the Do˜nana marshes using Landsat TM and ETM+ images. *Journal of the Environment Management.* 90(7) : 2219-2225.
- Campbell, P.K.E., Middleton, E.M., Corp, L.A. and Kim, M.S. 2008. Contribution of chlorophyll fluorescence to the apparent vegetation reflectance. *Sci. Total. Environ.* 404(2-3): 433-439.
- Chavez, P.S. 1988. An improved dark-object subtraction technique for atmospheric scattering correction of multispectral data. *Remote Sens. Environ.* 24(3): 459-479.
- Chen, Z., Muller-Karger, F.E. and Hu, C. 2007. Remote sensing of water clarity in Tampa Bay. *Remote Sens. Environ.* 109 (2) : 249-259.
- Choubey, V.K. 1992. Correlation of turbidity with Indian Remote Sensing Satellite-1A data. *Hydrolog. Sci. J.* 37 (2) : 129-140.
- Cox, R.M. Jr., Forsythe, R.D., Vaughan, G.E. and Olmsted, L.L. 1998. Assessing water quality in Catawba River reservoirs using Landsat Thematic Mapper satellite data. *Lake and Reservoir Management.* 14(4): 405-416.
- Crane, R.B. 1971. Pre-processing techniques to reduce atmospheric and sensor variability in multi-spectral scanner data p.1345-1355. In: *Proceedings of the 7th International Symposium on Remote Sensing of Environment*. Ann Arbor: University of Michigan.
- Crippen, R.E. 1987. The regression intersection method of adjusting image data for band rationing. *Int. J. Remote Sens.* 8(2): 137-155.
- Curran, P., Hansom, J., Plummer, S. and Pedley, M. 1987. Multispectral remote sensing of nearshore suspended sediments: A pilot study. *Int. J. Remote Sens.* 8 (1) : 103-112.
- Dekker, A.G. and Peters, S.W.M. 1993. The use of the

- Thematic Mapper for the analysis of eutrophic lakes: a case study in the Netherlands. *Int. J. Remote Sens.* 14 (5): 799-821.
- Dekker, A.G., Vos, R.J. and Peters, S.W.M. 2001. Comparison of remote sensing data, model results and in situ data for total suspended matter (TSM) in the southern Frisian lakes. *Sci. Total Environ.* 268(1-3) : 197-214.
- Dekker, A.G., Vos, R.J. and Peters, S.W.M. 2002. Analytical algorithms for lake water TSM estimation for retrospective analyses of TM and SPOT sensor data. *Int. J. Remote Sens.* 23(1) : 15-35.
- Doxaran, D., Froidefond, J.M., Castaing, P. and Babin, M. 2009. Dynamics of the turbidity maximum zone in a macrotidal estuary (the Gironde, France): Observations from field and MODIS satellite data. *Estuar. Coast Shelf Sci.* 81(3) : 321-332.
- Duan, W., Takara, K., He, B., Luo, P., Nover, D. and Yamashiki, Y. 2013. Spatial and temporal trends in estimates of nutrient and suspended sediment loads in the Ishikari river, Japan, 1985 to 2010. *Sci. Total Environ.* 461-462: 499-508.
- Duane Nellis, M., Harrington, J.J.J.A. and Wu, J. 1998. Remote sensing of spatial and temporal variations in pool size, suspended sediment, turbidity and Secchi depth in Turtle Creek Reservoir, Kansas: 1993. *Geomorphology.* 21 (3-4) : 281-293.
- Eaton, A.D., Clęsceri, L.S., Rice, E.W., Greenberg, A.E. and Franson, M.A.H. 2005. Standard methods for the examination of water and wastewater. American Public Health Association, Washington DC.
- Feng, L., Hu, C., Han, X., Chen, X. and Qi, L. 2014. Long-term distribution patterns of chlorophyll-a concentration in China's largest freshwater lake: MERIS full-resolution observations with a practical approach. *Remote Sensing.* 7(1) : 275-299.
- Fraser, R.N. 1998. Multispectral remote sensing of turbidity among Nebraska Sand Hills lakes. *Int. J. Remote Sens.* 19(15): 3011-3016.
- Gholizadeh, M.H., Melesse, A.M. and Reddi, L. 2016. A Comprehensive Review on Water Quality Parameters Estimation Using Remote Sensing Techniques. *Sensors.* 16 (8) : 1298.
- Giardino, C., Pepe, M., Brivio, P.A., Ghezzi, P. and Zilioli, E. 2001. Detecting chlorophyll, Secchi disk depth and surface temperature in a sub-alpine lake using Landsat imagery. *Sci. Total Environ.* 268(1-3) : 19-29.
- Gomez, F., Gorsky, G., Garcia-Gorriz, E. and Picheral, M. 2004. Control of phytoplankton distribution in the Strait of Gibraltar by winds and fortnightly tides. *Estuar. Coast Shelf Sci.* 59 (3) : 485-497.
- Goodin, D.G., Harrington, Jr, J.A., Duane Nellis, M. and Rundquist, D.C. 1996. Mapping Reservoir Turbidity Patterns Using SPOTHRV Data. *Geocarto Int.* 11 (4) : 71-78.
- Haddad, K.D. and Harris, B.A. 1985. Use of remote sensing to assess estuarine habitats. In: Magoon, O., Converse, H., Miner, D., Clark, D. and Tobin, L (eds) *Coastal Zone '85*. American Society of Civil Engineers, New York.
- Hadjimitsis, D.G. 1999. The application of atmospheric correction algorithms in the satellite remote sensing of reservoirs. PhD Thesis, University of Surrey.
- Hadjimitsis, D.G., Clayton, C.R.I. and Hope, V.S. 2004a. An assessment of the effectiveness of atmospheric correction algorithms through the remote sensing of some reservoirs. *Int. J. Remote Sens.* 25(18) : 3651-3674.
- Hadjimitsis, D.G., Clayton, C.R.I. and Retalis, A. 2004b. On the darkest pixel atmospheric correction algorithm: A revised procedure applied over satellite remotely sensed images intended for environmental applications. In: *Proceedings 10th International Symposium on Remote Sensing, Spain*.
- He, W., Chen, S., Liu, X. and Chen, J. 2008. Water quality monitoring in a slightly-polluted inland water body through remote sensing-case study of the Guanting Reservoir in Beijing, China. *Frontiers of Environmental Science & Engineering in China.* 2(2): 163-171.
- Hu, C., Chen, Z., Clayton, T.D. and Swarzenski, P., Brock, J.C. and Muller-Karger, F.E. 2004. Assessment of estuarine water-quality indicators using MODIS medium- resolution bands: initial results from Tampa Bay, FL. *Remote Sens. Environ.* 93 (3) : 423-441.
- IOCCG 2006. Remote Sensing of Inherent Optical Properties: Fundamentals, Tests of Algorithms, and Applications. In: Lee, Z.P. edited, *Reports of the International Ocean-Colour Coordinating Group*, Canada.
- Irons, J.R. and Loveland, T.R. 2013. Eighth Landsat satellite becomes operational. *Photogrammetric Engineering and Remote Sensing.* 79 (2013) : 398-401.
- Jensen, J.R. 2000. *Remote Sensing of the Environment: An Earth Resource Perspective*. Prentice Hall, New Jersey.
- Keith, D.J., Schaeffer, B.A., Lunetta, R.S., Gould, R.W., Rocha, K. and Cobb, D.J. 2014. Remote sensing of selected water-quality indicators with the hyperspectral imager for the coastal ocean (HICO) sensor. *Int. J. Remote Sens.* 35 (9) : 2927-2962.
- Khorram, S., Cheshire, H., Geraci, A.L. and Rosa, G.L. 1991. Water quality mapping of Augusta Bay, Italy from Landsat-TM data. *Int. J. Remote Sens.* 12: 803-808.
- Khorram, S. and Cheshire, H.M. 1985. Remote sensing of water quality in the Neuse river estuary, North Carolina. *Photogramm. Eng. Rem. S* 51 (3) : 329-341.
- Kirk, J.T.O. 1994. *Light and Photosynthesis in Aquatic Ecosystems*. NY7 Cambridge University Press,

- New York.
- Kloiber, S.M., Brezonik, P.L., Olmanson, L.G. and Bauer, M.E. 2002. A procedure for regional lake water clarity assessment using Landsat multispectral data. *Remote Sens. Environ.* 82(1): 38-47.
- Lathrop, R. 1992. Landsat thematic mapper monitoring of turbid inland water quality. *Photogramm. Eng. Rem. 58* : 465-470.
- Lathrop, R.G. Jr. and Lillesand, T.M. 1989. Monitoring water quality and river plume transport in Green Bay, Lake Michigan with SPOT-1 imagery. *Photogramm. Eng. Rem.* 55 : 349-354.
- Lavery, P., Pattiaratchi, C., Wyllie, A. and Hick, P. 1993. Water quality monitoring in estuarine waters using the landsat thematic mapper. *Remote Sens. Environ.* 46 (3) : 268-280.
- Li, J. and Sheng, Y. 2012. An automated scheme for glacial lake dynamics mapping using Landsat imagery and digital elevation models: A case study in the Himalayas. *Int. J. Remote Sens.* 33(16): 5194-5213.
- Lim, J. and Choi, M. 2015. Assessment of water quality based on Landsat 8 operational land imager associated with human activities in Korea. *Environ. Monit. Assess.* 187 : 384.
- Liversedge, L.K. 2007. Turbidity mapping and prediction in ice marginal lakes at the Bering Glacier system, Alaska. MS Thesis, University of Michigan.
- Lopez-Garcia, M.J. and Caselles, V. 1987. Use of Thematic Mapper data to assess water quality in Albufera Lagoon of Valencia (Spain) p.510-519. In: *Advances in digital image processing. Remote Sensing Society*, Nottingham.
- McHugh, M.L. 2008. Standard error: meaning and interpretation. *Biochemia Medica.* 18 (1) : 7-13.
- Miller, H.M., Richardson, L., Koontz, S.R., Loomis, J. and Koontz, L. 2013. Users, uses, and value of Landsat satellite imagery-Results from the 2012 survey of users. U.S. Geological Survey Open-File Report 2013-1269.
- Miller, R.L. and McKee, B.A. and D'Sa, E.J. 2005. Monitoring bottom sediment resuspension and suspended sediments in shallow coastal waters p.259-276. In: Muller, R.L., Del Castillo, C.E. and McKee, B.A. edited. *Remote Sensing of Coastal Aquatic Environments*. Springer, Dordrecht.
- Mobley, C.D. 1994. *Light and water: Radiative transfer in natural waters*. CA7 Academic Press, San Diego.
- Nechad, B., Ruddick, K. and Park, Y. 2010. Calibration and validation of a generic multisensor algorithm for mapping of total suspended matter in turbid waters. *Remote Sens. Environ.* 114 (4) : 854-866.
- Novo, E., Hansom, J. and Curran, P. 1989. The effect of viewing geometry and wavelength on the relationship between reflectance and suspended sediment concentration. *Int. J. Remote Sens.* 10(8): 1357-1372.
- Papoutsas, C., Retalis, A., Toullos, L. and Hadjimitsis, D.G. 2014. Defining the Landsat TM/ETM+ and chris/proba spectral regions in which turbidity can be retrieved in inland water bodies using field spectroscopy. *Int. J. Remote Sens.* 35 : 1674-1692.
- Patra, P.P., Dubey, S.K., Trivedi, R.K., Sahu, S.K. and Rout, S.K. 2017. Estimation of chlorophylla concentration and trophic states in Nalban Lake of East Kolkata Wetland, India from Landsat 8 OLI data. *Spat. Inf. Res.* 25 (1) : 75-87.
- Petous, C., Chust, G., Gohin, F., Doxaran, D., Froidefond, J.M. and Sagarmínaga, Y. 2010. Estimating turbidity and total suspended matter in the Adour River plume (South Bay of Biscay) using MODIS 250-m imagery. *Cont. Shelf. Res.* 30 (5): 379-392.
- Ritchie, J.C., Schiebe, F.R. and McHenry, J.R. 1976. Remote Sensing of Suspended Sediments in Surface Water. *Photogramm. Eng. Remote Sensing.* 42 (2) : 1539-1545.
- Ritchie, J.C., Cooper, C.M. and Yongquing, J. 1987. Using Landsat multispectral scanner data to estimate suspended sediments in Moon Lake, Mississippi. *Remote Sens. Environ.* 23 (1) : 65-81.
- Roy, D.P., Wulder, M.A., Wulder, T.R., Allen, X.R.G., Anderson M.C., Helder, D. and Irons, J.R. 2014. Landsat-8: Science and product vision for terrestrial global change research. *Remote Sens. Environ.* 145 : 154-172.
- Sass, G.Z., Creed, I.F., Bayley, S.E. and Devito, K.J. 2007. Understanding variation in trophic status of lakes on the Boreal Plain: A 20 year retrospective using Landsat TM imagery. *Remote Sens. Environ.* 109(2) : 127-141.
- Scheffer, M. 1998. *Ecology of Shallow Lakes*. Chapman & Hall, London.
- Sheng, Y. and Li, J. 2011. Satellite-observed endorheic lake dynamics across the Tibetan Plateau between circa 1976 and 2000 p. 305-319. In: Wang, Y.Q. (ed), *Remote Sensing of Protected Lands*. CRC Press, New York.
- Smith, L.C., Sheng, Y., MacDonald, G.M. and Hinzman, L.D. 2005. Disappearing Arctic Lakes. *Science.* 308 (5727) : 1429.
- Sudheer, K.P., Chaubey, I. and Garg, V. 2006. Lake water quality assessment from Landsat thematic mapper data using neural network: an approach to optimal band combination selection. *J. Am. Water Resour. Assoc.* 42 (6) : 1683-1695.
- Tassan, S. 1997. A numerical model for the detection of sediment concentration in stratified river plumes using Thematic Mapper data. *Int. J. Remote Sens.* 18 (12) : 2699-2705.
- Topliss, B.J., Almos, C.L. and Hill, P.R. 1990. Algorithms for remote sensing of high concentration, inorganic suspended sediment. *Int. J. Remote Sens.* 11(6): 947-966.
- Udy, J., Gall, M., Longstaff, B., Moore, K., Roelfsoma, C.,

- Spooner, D.R. and Albert, S. 2005. Water quality monitoring: a combined approach to investigate gradients of change in the Great Barrier Reef, Australia. *Mar. Pollut. Bull.* 51(1-4) : 224-238.
- Wang, C., Li, D., Wang, D., Shuisen, C. and Lie, W. 2016. A total suspended sediment retrieval model for multiple estuaries and coasts by Landsat imageries. *Fourth International Workshop on Earth Observation and Remote Sensing Applications (EORSA)*.
- Wang, Y., Xia, H., Fu, J. and Sheng, G. 2004. Water quality change in reservoirs of Shenzhen, China: detection using Landsat/ TM data. *Sci. Total Environ.* 328 (1-3) : 195-206.
- Wass, P., Marks, S., Finch, J., Leeks, G.J.L. and Ingram, J. 1997. Monitoring and preliminary interpretation of in-river turbidity and remote sensed imagery for suspended sediment transport studies in the humber catchment. *Sci. Total Environ.* 194 : 263-283.
- Wu, J., Wang, D. and Bauer, M.E. 2005. Image-based atmospheric correction of QuickBird imagery of Minnesota Cropland. *Remote Sens. Environ.* 99 (3): 315-325.
- Yuming, Y. and Min, H. 1992. Remote sensing analysis of the suspended sediment transport in Lingdingyang. *China Ocean Eng.* 6 (3) : 331-349.
- Zhou, W., Wang, S., Zhou, Y. and Troy, A. 2006. Mapping the concentrations of total suspended matter in Lake Taihu, China, using Landsat 5 TM data. *Int. J. Remote Sens.* 27 (6) : 1177-1191.
-